NASA

Technical Memorandum 80724

Thermal Structure and Dynamics of the Jovian Atmosphere
II. Visible Cloud Features

B.J. Conrath, F.M. Flasar, J.A. Pirraglia,
P.J. Gierasch and G.E. Hunt

NOVEMBER 1980

National Aeronautics and
Space Administration

Goddard Space Flight Center
Greenbelt, Maryland 20771

THERMAL STRUCTURE AND DYNAMICS OF THE JOVIAN ATMOSPHERE
II. VISIBLE CLOUD FEATURES

B.J. CONRATH, F.M. FLASAR, J.A. PIRRAGLIA
Goddard Space Flight Center
Greenbelt, MD. 20771

P.J. GIERASCH
Cornell University
Ithaca, NY 14853

G.E. HUNT
University College London
London, England

June 1980
Revised November 1980

Abstract

Investigation of the thermal structure above selected cloud features in the Jovian atmosphere, making use of Voyager IRIS data, reveals strong similarities among a broad range of features which differ considerably in visual appearance. The atmosphere above anticyclonic features, including the major white ovals, the Great Red Spot, and a zone, are cold relative to the immediate surroundings in the upper troposphere and tropopause region. These results are consistent with upwelling and divergence in this part of the atmosphere. In contrast a "hot spot" and a "barge", which are localized cyclonic features, are found to be warm relative to their surroundings, implying subsidence with accompanying convergence. In all cases, the thermal wind shear associated with the features indicates a decay of the vorticity with height in the upper troposphere and lower stratosphere. Vertical velocities inferred from the observed temperature perturbations imply an upper limit of vertical mixing times near the tropopause of $\sim$ 20 years. Temperatures in the upper stratosphere above the anticyclonic features show considerable variation, but in most cases are found to be relatively warm. At the present time no satisfactory explanation for this behavior appears to exist.

Introduction

The atmosphere of Jupiter displays a wide variety of cloud features including the planetary scale belt-zone system, long lived spots and ovals, plumes, and smaller scale structure extending down to the resolution limit of the Voyager images. A major objective of current work on the Jovian atmosphere is to achieve an understanding of the relationship of these features to one another and to the basic dynamic regime. Similarities in the dynamic properties of certain types of cloud features have long been recognized from ground based observations of cloud motion (see for example Peek, 1958). The zones and the Great Red Spot (GRS) display anticyclonic vorticity and must therefore be regions of high pressure, probably accompanied by upwelling and divergence as first discussed by Hess and Panofsky (1951). The existence of high pressure at the level of visible motion implies that the feature must be warm relative to its surroundings along constant pressure surfaces somewhere below this level. The rising motion associated with such systems is expected to result in a relatively high, well developed cloud structure. This picture is supported by a variety of observational evidence including measurements of 5-μm emission (Terrile, et al., 1979), Pioneer photopolorimeter measurements (Gehrels, 1976), and ground-based photometry in near-infrared CH_4 bands (West and Tomasko, 1980). In contrast the belts are apparently regions of cyclonic vorticity with sinking motion and low, less well developed clouds.

The Voyager encounters with Jupiter have now provided a wealth of new data on the cloud features. In addition to the extensive imaging data, spatially resolved infrared spectra from the IRIS instrument (Hanel, et al. 1979a; 1979b) can provide information on the thermal structure of the atmosphere above some of the features. Because of the relatively large spatial dimensions of the Great Red Spot (GRS), it was possible to resolve its internal thermal structure, and a detailed investigation of this feature has been carried out (Flasar, et al. 1981, hereafter referred to as Paper I). It is the purpose of the present paper to extend the investigation of thermal structure to include other cloud features in order that the comparison of the dynamic properties of the features may be further pursued.

The features examined here include the major white ovals, "hot spot" regions of strong 5-um emission, the dark brown elongated features dubbed "barges", and a belt-zone pair. The available spatial resolution of the IRIS data permits only the gross thermal structure of most of the features to be obtained; nevertheless, interesting comparisons among the features can be made.

In the following section the observations are presented, and the limitations on the data are discussed. The implications of the observed thermal structure in the upper troposphere and lower stratosphere are then considered in terms of the vorticity of the features, the implied vertical motion fields, and vertical mixing. Next the thermal structure of the upper stratosphere is discussed, and various possible models are examined, including radiative heating, vertical wave propagation, and thermally indirect merdional cells. Finally, conclusions are drawn concerning the dynamical similarities and differences of the various features.

Observations

Using the Voyager images, examples of specific Jovian cloud features have been selected, and simultaneously acquired infrared spectra have been inverted to obtain vertical temperature profiles. The methods employed and their limitations have been discussed in detail by Conrath and Gautier (1979) and are summarized briefly in Paper I. In the troposphere (below ~100 mb) a vertical resolution ranging from 0.5 to 1 pressure scale height is obtained. The information content of the measurements above the tropopause is relatively poor, especially in the lower stratosphere. Thus, detailed vertical structure in the stratosphere is inaccessable, and only the gross features may be inferred.

The field of view of the IRIS instrument projected onto the planet is in most cases comparable to the horizontal dimensions of the features which are being studied and only the mean temperature structure over each feature can be retrieved. As noted above, an exception is the Great Red Spot. For purposes of this study we are concerned primarily with the local perturbation in the temperature field associated with a given feature so temperature profiles from the regions immediately surrounding the feature have been averaged and

subtracted from the mean profile directly over the feature. The resulting temperature differences as functions of pressure level are shown for several features in Figs. 1, 2 and 3. The formal error in these temperature differences, considering only the propagation of instrumental noise, is about ±1K between the 500 and 100 mb levels, and increases in the stratosphere to ±5K at the 2 mb level.

The three major white ovals, designated in Fig. 1 as FA, BC, and DE, show relatively cold regions in the upper troposphere and lower stratosphere, while there is considerable variation among the features in the upper stratosphere. The behavior of the retrieved thermal structure immediately above the 500 mb level may be due to cloud or haze opacity effects which were not taken into account in the analysis. However, in the upper troposphere and lower stratosphere, the results appear to be due to real temperature depressions above the ovals. The visual appearances of these features, which apparently began to form in about 1939 (Peek, 1958), have been extensively documented in Earth-based observations. They currently appear as high albedo features with an east-west dimension of 12,000 km (Beebe and Youngblood, 1979), and Voyager imaging indicates they possess anticyclonic vorticity at the visible cloud top level.

The difference between the mean temperature over the GRS and its surroundings is shown in Fig. 2 along with the temperature difference between a zone and belt. The latter temperature difference was obtained from data over the North Tropical Zone near 20°N and the North Equatorial Belt near 15°N. The atmosphere above both the GRS and the zone (relative to the belt) is cold in the upper troposphere and lower stratosphere similar to that above the white ovals. These features also display anticyclonic vorticity in common with the ovals. On the other hand, the upper stratosphere above both features is relatively warm. Warm regions in the stratosphere over zones have also been detected in ground based observations (Caldwell, et al., 1979; Cess, et al., 1980).

Differences in temperature above a 5-μm hot spot and a barge relative to their surroundings are shown in Fig. 3. In contrast to the features previously discussed, the upper troposphere and tropopause are warm relative

to the immediate surroundings. The hot spots have been extensively observed using ground based techniques (see, for example, Terrile and Westphal, 1977), and regions of strongest emission are found to be highly localized. The particular feature considered here was located at approximately 9°N just to the east of one of the plume heads discussed by Hunt, et al. (1980). The blue color observed in images of features such as this is consistent with the absence of significant upper level clouds and with considerable sensing of deeper atmospheric layers. The brightness temperature near 2000 cm^{-1} in the IRIS spectrum of this feature is about 250 K.

Barge features were observed in Pioneer 10 and 11 images and have also been observed at 5-μm where they appear warm relative to their surroundings (Terrile and Beebe, 1979), but they are generally less warm than the hot spots. The IRIS data indicate that the particular barge considered here has a brightness temperature near 2000 cm^{-1} of 235 K. This fact along with the dark brown color of the feature indicates that barges are probably associated with a clearing in the upper layer clouds, but the clearing may not extend to depths as great as in the case of the hot spots. The feature which is shown in a Voyager image in Fig. 4, is located near 15°N and displays a cyclonic vorticity at the cloud tops (Smith, et al. 1979a). The superposed IRIS field of view indicates that some of the areas to the immediate north and south of the barge are averaged into the thermal structure over the feature, so it is probable that the actual temperature increment may be somewhat larger than indicated by this analysis. Similarly, the thermal contrast obtained above the hot spot may also be underestimated since the region of strongest 5-μm emission may be smaller than the instrument field of view.

Discussion

The observations suggest strong similarities in the thermal structure above a large class of cloud features. Temperature perturbations in the upper troposphere and in some cases the upper stratosphere reflect the presence of these features. The possible implications of the temperature structure in the upper troposphere and tropopause region will be considered first.

The data indicate that anticyclonic features are correlated with a cold tropopause region and relatively low 5-μm temperatures. As noted above, the 5-μm temperatures serve as indicators of the presence or absence of high clouds while the thermal structure at the tropopause level presumably corresponds to actual atmospheric temperature differences along constant pressure surfaces. Assuming that horizontal pressure gradients vanish at some level in the deep atmosphere, the high pressure associated with anticyclonic vorticity then requires the existence of warm layers below the cloud tops. Thus, the sign of the temperature perturbation must change somewhere below the levels sounded by the IRIS data. The results shown in Figs. 1 and 2 do indicate a gross trend in this sense at the lowest levels sounded; however, possible cloud opacity effects prevent a definite conclusion on this point. The data for the cyclonic features considered here indicate a relatively warm tropopause regions. The associated low pressure again requires a change in sign of the perturbation, in this case with relatively cold temperatures occurring somewhere below the region sounded with the IRIS data.

In all cases the observed horizontal temperature gradients are in the correct sense to produce a thermal wind shear (see for example Holton, 1972) which will reduce the vorticity with increasing height. Thus, we are seeing a decay of the wind systems in the upper troposphere and lower stratosphere. An example of this effect is shown in Fig. 5 where the thermal wind has been calculated from the belt-zone temperature gradient displayed in Fig. 2. The required lower boundary condition was taken to be the $\sim$30 m s^{-1} wind speed obtained from the Voyager imaging data for the easterly jet at 18°N which lies on the interface of the belt-zone pair to which the temperature data pertain (Ingersoll, et al. 1979). Although the atmospheric pressure level of the wind derived from the images is not known with certainty, for purposes of this calculation it was assigned to the 500 mb level. The decay of the jet in the lower stratosphere is similar in behavior to the decay of the GRS vortex described in Paper I. Other examples of thermal winds associated with zonal jets have been given by Allison, et al. (1979).

One possible explanation of the observed tropopause structure is radiative control. Horizontal variations in cloud top heights and in

radiative fluxes would tend to produce horizontal contrasts in temperature. Consistent with this hypothesis are IRIS observations that total infrared fluxes from regions with warm tropopauses are 10 - 20% greater than those from areas with cold tropopauses. Such a model, however, would predict that maximum thermal contrasts occur near the cloud tops, rather than at the tropopause, as is observed. Moreover, comparison of the tropopause thermal structure from Voyager 1 and 2 IRIS data (Hanel et al., 1979b) has revealed changes in this structure over a four-month interval. This suggests that the tropopause is dynamically controlled to a significant degree, because the radiative relaxation time at this level is $\gtrsim$ 3 years.

Another possible explanation for the cold regions is adiabatic cooling associated with uplifting of atmospheric parcels above the anticyclonic features. A simplified model which is consistent with the observed thermal structure is discussed in the Appendix. Although the energy source required to drive the system is not explicitly specified, one possibility is latent heat release (Barcilon and Gierasch, 1970; Ingersoll, 1975) as discussed in detail in Paper I. The model treats an isolated, axisymmetric, steady vortex in which the tangential flow is geostrophically balanced and radial motions are frictionally controlled. If friction is represented by a linear (Rayleigh) damping term, then a high pressure core and the attendant anticyclonic vorticity imply diverging motions (see eqs. (A.7) and (A.8)). Thus, for example, we would expect divergence to occur within the GRS and white ovals from below the visible cloud tops up to the lower stratosphere, the region over which anticyclonic vorticity is observed to exist. Conversely, at similar atmospheric levels convergence would be implied over cyclonic features such as the barges. In the absence of local sources of heat or momentum, the natural vertical scale for decay predicted by the model is

$$D = P^{-1/2} \frac{f}{N} L \qquad (1)$$

where f is the Coriolis frequency ($\simeq$ 1.8 x 10^{-4} at a latitude of 30°), N is the horizontal mean Brunt-Vaisala frequency ($\simeq$.023 s^{-1} at the tropopause), L is the horizontal scale of the vortex, and P is the ratio of the time scale for radiative thermal damping to that for momentum damping. If L is taken as the mean vortex radius, then for a feature 10^4 km in diameter, D $\simeq$ 1.5 scale heights. From Figs. 1,2 and 3, this value

of D is consistent with the vertical scale of the perturbations in the lower stratosphere when P ≈ O(1). However, because of the limited information content of the measurements in the lower stratosphere, the observed vertical scale represents essentially an upper limit on the true scale.

Horizontal variations in temperature are maintained in the absence of diabatic heating by the adiabatic heating and cooling associated with vertical motion (Eq. (A.11)). In dimensional form, this becomes:

$$w \left(\frac{dT_o}{dz} + \frac{\kappa T_o}{H} \right) \approx -\sigma_k T, \tag{2}$$

where w is vertical velocity, $dT_o/dz + \kappa T_o/H$ is the mean static stability, σ_k is a thermal damping constant, and T is the local departure of temperature from the horizontal mean, T_o. Both radiation and small-scale turbulence are assumed to smooth out local variations in temperature and produce a horizontally uniform state (T_o). Eq. (2) can be used to estimate w at the tropopause over various features. The magnitude of the turbulent exchange of heat is not well known, but a lower limit to the thermal damping constant is given by the radiative damping rate: $\sigma_k \gtrsim 10^{-8}$ s^{-1} (Gierasch and Goody, 1969). The static stability is $\gtrsim 2 \times 10^{-5}$ K cm^{-1} at the tropopause. Estimates of T follow from Figs. 1 and 2. For the GRS, T ≈ 9 K and $w \gtrsim .0045$ cm s^{-1}. From the scaling of the mass continuity equation, the corresponding diverging radial velocities are found to be of the order of 1 cm s^{-1}. It is perhaps not surprising that Smith, et al. (1979) were unable to detect radial motions within the GRS. The vertical mixing time (D/w) associated with these estimates is approximately 20 years for the lower stratosphere. This is less than the 300 year mixing time scale corresponding to an eddy diffusivity of 10^3 cm^2 s^{-1} at the tropopause which has been used in the photochemical models of Strobel (1977), Strobel and Yung (1978), and Yung and Strobel (1980). However, the possibility that vertical motions decay rapidly in the lower stratosphere cannot be ruled out because of the limited vertical resolution of the temperature retrieval in this part of the atmosphere.

If the tropopause structure is determined everywhere by (2) then thermal maps of the tropopause, such as the 602 cm^{-1} maps presented by Hanel et al. (1979b), can be interpreted as maps of vertical motion. It should be noted, however, that temperature perturbations above Jovian features may not be directly indicative of local vertical velocities in all cases. For example air parcels may follow streamlines in a wave crest and experience adiabatic cooling; if diabatic processes are neglected the temperature perturbation then reflects the total vertical displacement rather than the rate of displacement. One example of this type is the solitary wave model of the GRS suggested by Maxworthy and Redekopp (1976). In this model the vortex is viewed as a feature located in the statically stable portion of the atmosphere with little penetration below the ammonia cloud level. However, as discussed in Paper I, the model does not naturally explain the detailed thermal structure observed above the GRS at the tropopause level. Moreover, the ring of 5-μm emission surrounding the GRS appears to indicate a relatively deep penetration of the dynamic system associated with this feature. The strong 5-μm emission from the cyclonic features indicates that these must also be relatively deep systems with downward motion penetrating to somewhat greater depths in the hot spot than in the barge.

The upper stratospheric thermal structure associated with the GRS, ovals, and belt-zone system cannot be explained in terms of the simplified dynamical model used in the discussion of the upper troposphere and lower stratosphere; therefore, an alternate explanation must be sought. One possible mechanism is the vertical propagation of the long wave components of the quasi-geostrophic wave spectrum associated with the feature. However, as discussed in Paper I, an application of linear wave propagation theory leads to predictions of an east-west asymmetry in the perturbation isotherms which are inconsistent with observations in the case of the GRS.

A possible explanation for the warm upper stratosphere over zones has been suggested by Cess, et al. (1980). The absorption in the upper stratosphere of backscattered solar radiation from the high albedo zones

is invoked. Such a source of differential diabatic heating would clearly have a strong influence on the dynamic behavior of this part of the atmosphere. Presumably a thermally direct circulation would be induced which would tend to decrease the horizontal temperature gradients, but the radiative-dynamic balances required to maintain such a system have not been investigated.

Still another possible explanation invokes the forcing of a thermally indirect cell in the stratosphere which would account for the observed thermal structure through adiabatic heating and cooling associated with vertical motion. Such an indirect cell might be driven by either the continuation into the stratosphere of a thermally direct tropospheric cell or by convergence of eddy momentum flux associated with waves propagating from below. Again no quantitative models for these mechanisms yet exist.

Summary and Conclusions

Investigation of the atmospheric temperatures above the major white ovals and a zone indicates that the gross thermal structure associated with these features is qualitatively similar to that of the GRS which was analyzed in detail in Paper I. Thus, these results provide additional evidence in support of the view that these anticyclonic features are indeed manifestations of similar dynamic processes, differing primarily in geometric symmetry. The observed cold upper troposphere and tropopause is consistent with adiabatic cooling resulting from forced upward motion and accompanying divergence. In contrast the cyclonic barge and hot spot features show a warm upper troposphere and tropopause consistent with adiabatic heating accompanying subsidance and convergence. If it is assumed that adiabatic heating and cooling near the tropopause are balanced by thermal damping, then an upper limit of $\sim$ 20 years is implied for the mixing time in this region of the atmosphere.

The thermal wind shear implied by the observed temperature gradients indicates the vorticity associated with all of the features decays with height in the upper troposphere and lower stratosphere. This behavior is

well described by a frictionally controlled vortex model. While the nature of the energy source required to drive such a model cannot be inferred directly from the data, latent heat release at the water cloud level is a likely candidate.

The upper stratosphere is found to be relatively warm in most cases above the anticyclonic features. At the present time, no completely satisfactory explanation for this phenomenon exists.

Acknowledgement

The authors are indebted to R. A. Hanel for discussions during the course of this work.

Appendix: Frictionally Controlled Axisymmetric Steady Vortex

We consider the governing equations for an axisymmetric, steady vortex with Rayleigh friction and Newtonian cooling. The following notation is employed:

r,z	radial and vertical (log-pressure) coordinates
H	scale height, assumed constant
R	gas constant for a dry atmosphere
C_p	specific heat at constant pressure
κ	$= R/C_p$
f	Coriolis frequency
u,v,w	azimuthal, radial, and vertical velocities
$\phi_o(z),T_o(z)$	horizontally averaged geopotential and temperature
ϕ,T	departure of geopotential and temperature from their horizontal averages
N	the mean Brunt-Vaisala frequency, $= \frac{R}{H}\left(\frac{dT_o}{dz} - \frac{\kappa T_o}{H}\right)^{1/2}$, assumed constant
σ_v	frictional damping constant
σ_k	thermal damping constant
D,L	characteristic vertical and horizontal scales of motion
U	characteristic azimuthal velocity
μ	$= D/H$

Ro — the Rossby number = $U (f L)^{-1}$

E — an Ekman number = σ_ν / f

ϵ — the Burger number = $\frac{N^2 D^2}{f^2 L^2}$

P — a Prandtl number = σ_ν / σ_k

In the absence of sources of heat or momentum, the equations of motion on an f-plane are (see for example, Holton, 1975)

$$v\,\partial_r u + w\,\partial_z u + \frac{uv}{r} = -fv - \sigma_\nu u, \tag{A.1}$$

$$v\,\partial_r v + w\,\partial_z v - \frac{u^2}{r} = fu - \partial_r \phi - \sigma_\nu u, \tag{A.2}$$

$$\partial_z \phi_o = \frac{RT_o}{H} \qquad \partial_z \phi = \frac{RT}{H} \tag{A.3}$$

$$\frac{1}{r}\,\partial_r (rv) + \partial_z w - \frac{w}{H} = 0, \tag{A.4}$$

$$v\,\partial_r T + w\left(\partial_z T + \frac{\kappa T}{H} + \frac{dT_o}{dz} + \frac{\kappa T_o}{H}\right) = -\sigma_\kappa T \tag{A.5}$$

Diabatic heating, such as that from latent heat release, can be included by adding the appropriate parameterized source term to the right-hand side of (A.5).

We choose a particular set of scalings for the dynamical variables, the consequences of which we will discuss below. Choose non-dimensional (primed) variables as follows:

$$r = Lr', \; z = Dz', \; u = Uu', \; v = EUv'$$
$$w = \frac{D}{L} E\, U\, w', \; \phi = f\, L\, U\, \phi', \; T = \frac{fL}{\mu R}\, U\, T', \tag{A.6}$$

The resulting nondimensional equations are

$$Ro\left(v'\,\partial_{r'} u' + w'\,\partial_{z'} u' + \frac{u'v'}{r'}\right) = \underline{-v' - u'} \tag{A.7}$$

$$E\,\lambda_o\,(v'\,\partial_{r'}\,v' + w'\,\partial_{z'}v') - Ro\,\frac{u'^2}{r'} = \underline{-\partial_{r'}\phi' + u'} - E^2 v' \qquad (A.8)$$

$$\underline{\partial_{z'}\phi' = T'} \qquad (A.9)$$

$$\underline{\frac{1}{r'}\,\partial_{r'}(r'v') + \partial_{z'}w' - \mu w' = 0} \qquad (A.10)$$

$$Ro[v'\,\partial_{r'}T' + w'\,(\partial_{z'}T' + \mu\,\kappa\,T')] + \underline{\epsilon\,w' = -P^{-1}\,T'} \qquad (A.11)$$

In order to make use of (A.6) - (A.11) it is necessary to specify the magnitudes of the dimensionless parameters Ro, E, ϵ, μ, and P. Observed cloud velocities (Smith et al. 1979a,b) imply Ro = $O(10^{-1})$ for the Great Red Spot, white ovals, and zone-belt systems. For the GRS, ϵ = 0.6 at the tropopause (Paper I) and values of O(1) pertain to the other localized features and the zone-belt circulation. The vertical scales of these features are not known; however, if the latent heat of water vapor plays an important role in this dynamics, D = $O(10^2 km)$ (Paper I) and hence μ = O(1). Little is known of the magnitude of small-scale momentum exchange in Jupiter's atmosphere, but E << 1 implies eddy diffusion coefficients << 10^9 - 10^{10} $cm^2\ s^{-1}$ at the tropopause, which seems reasonable. The lack of knowledge about turbulent heat and momentum exchange leave the value of P open to question. In this work we use

$$Ro,\ E \ll 1 \qquad \epsilon,\ \mu,\ P = O(1) \qquad (A.12)$$

The underlined terms in (A.7) - (A.11) denote the lowest order balances consistent with (A.6) and (A.12). Eq. (A.8) states that the tangential flow is geostrophically balanced, and (A.7) requires that Coriolis torques acting on the radial flow be nearly balanced by frictional damping on the azimuthal flow. Eqs. (A.9) and (A.10) are merely statements of hydrostatic balance and continuity, respectively. The heat equation, (A.11), states that the adiabatic heating and cooling associated with vertical motions act to maintain local variations in temperature against thermal damping.

The lowest-order balances in (A.7) - (A.11) can be combined to yield an equation in ϕ':

$$\frac{1}{r'}\,\partial_{r'}\,(r'\partial_{r'}\phi') + (\epsilon P)^{-1}\, e^{\mu z'}\,\partial_{z'}(e^{-\mu z'}\,\partial_{z'}\phi') = 0. \qquad (A.13)$$

With $\epsilon P = O(1)$ the natural vertical scale of the system is

$$D = P^{-1/2}\,\frac{f}{N}\,L \qquad (A.14)$$

While the above results were derived for cylindrically symmetric systems, similar physical considerations apply to the global, zonally symmetric belt-zone structure. In this case a meridional coordinate and meridional velocity replace the radial coordinate and radial velocity, and the horizontal length scale is associated with the latitudinal dimension of the belt-zone system.

References

Allison, M.D., B.J. Conrath, F.M. Flasar, J.A. Pirraglia, and G. Hunt, Zonal thermal winds on Jupiter from Voyager IRIS Bull Am. Astron. Soc., 11, 587, 1979.

Barcilon, A. and P. Gierasch, A moist, Hadley cell model for Jupiter's cloud bands, J. Atmos. Sci., 12, 550-560, 1970.

Beebe, R.F., and L.A. Youngblood, Pre-Voyager velocities, accelerations and shrinkage rate of Jovian cloud features, Nature, 280, 771-772, 1979.

Caldwell, J., R.D. Cess, B.E. Carlson, A.T. Tokunaga, F.C. Gillett, and I.G. Nolt, Temporal characteristics of the Jovian atmosphere, Astrophys. J., 234, L155-L158, 1979.

Cess, R.D., B.E. Carlson, J. Caldwell, I.G. Nolt, F.C. Gillett, and A.T. Tokunaga, Latitudinal variations in Jovian stratospheric temperature, to be published in Icarus, 1980.

Conrath, B.J., and D. Gautier, Thermal structure of Jupiter's atmosphere obtained by inversion of Voyager 1 infrared measurements, in Interpretation of Remotely Sensed Data edited by A. Deepak, Academic Press, New York, to be published, 1980.

Flasar, F.M., B.J. Conrath, J.A. Pirraglia, R. French, P. Clark, and P.J. Gierasch, Thermal structure and dynamics of the Jovian atmosphere. I. The Great Red Spot, J. Geophys. Res., this issue, 1981.

Gehrels, T., The results of the imaging photopolarimeter on Pioneers 10 and 11, in Jupiter, edited by T. Gehrels, The University of Arizona Press, Tucson, 1976.

Hanel, R., B. Conrath, M. Flasar, V. Kunde, P. Lowman, W. Maguire, J. Pearl, J. Pirraglia, R. Samuelson, D. Gautier, P. Gierasch, S. Kumar and C. Ponnamperuma, Infrared observations of the Jovian system from Voyager 1, Science, 204, 972-976, 1979a.

Hanel, R., B. Conrath, M. Flasar, L. Herath, V. LIA, R. Samuelson, D. Gautier, P. Gierasch, L. Horn, S. Kumar, and C. Ponnamperuma, Infrared observations of the Jovian system from Voyager 2, Science, 206, 952-956, 1979b.

Hess, S.L., and H.A. Panofsky, The atmospheres of the other planets, in Conpendium of Meteorology, T.F. Malone, ed., American Meteorological Society, Boston, 1951.

Holton, J.R. An Introduction to Dynamic Meteorology, Academic Press, New York, 1972.

Holton, J.R., The Dynamical Meteorology of the Stratosphere and Mesosphere, Amer. Met. Soc., Boston, 1975.

Hunt, G.E., B.J. Conrath and J.A. Pirraglia, Visible and infrared observations of Jovian plumes during the Voyager encounters, J. Geophys. Res., this issue, 1981.

Ingersoll, A.P., The atmosphere of Jupiter, Space Sci. Rev., 18, 603-639, 1976.

Ingersoll, A.P., R.F. Beebe, S.A. Collins, G.E. Hunt, J.L. Mitchell, P. Muller, B.A. Smith, and R.J. Terrile, Zonal velocity and texture in the Jovian atmosphere from Voyager images, Nature, 280, 773-775, 1979.

Maxworthy, T. and L.G. Redekopp, A solitary wave theory of the Great Red Spot and other observed features in the Jovian atmosphere, Icarus, 29, 261-271, 1976.

Peek, B.M., The Planet Jupiter, Faber and Faber, London, 1958.

Smith, B.A., L.A. Soderblom, T.V. Johnson, A.P. I. cloud vertical structures for several axisymmetric bands and the Great Red Spot, Icarus, 41, 278-292, 1980.

Yung, Y.L., and D.F. Strobel, Hydrocarbon photochemistry and Lyman alpha albedo of Jupiter, Astrophys. J., in press, 1980.

Figure Captions

Fig. 1. Differences between mean temperature over white ovals and their immediate surroundings. The three features considered here are the largest white ovals observed in the Jovian atmosphere and are located at 34°S latitude.

Fig. 2. Differences between mean temperatures over the North Tropical Zone and the adjacent North Equatorial Belt. The differences between the mean temperatures over the Great Red Spot and its immediate surroundings are shown for comparison.

Fig. 3. Differences between temperatures over a "hot spot" and a "barge" and their immediate surroundings. The hot spot is a localized region of strong 5-μm emission located at 9°N, while the barge is an elongated feature near 15°N.

Fig. 4. Voyager image of a portion of the barge feature to which the data shown in Fig. 3 pertain. The IRIS field of view is superposed on the image.

Fig. 5. Thermal winds calculated from the belt-zone temperature difference shown in Fig. 2. The wind field corresponds approximately to the retrograde jet located near 18°N. The lower boundary condition was taken as the wind velocity for this region inferred from Voyager images and assumed to pertain to the 500 mb level.

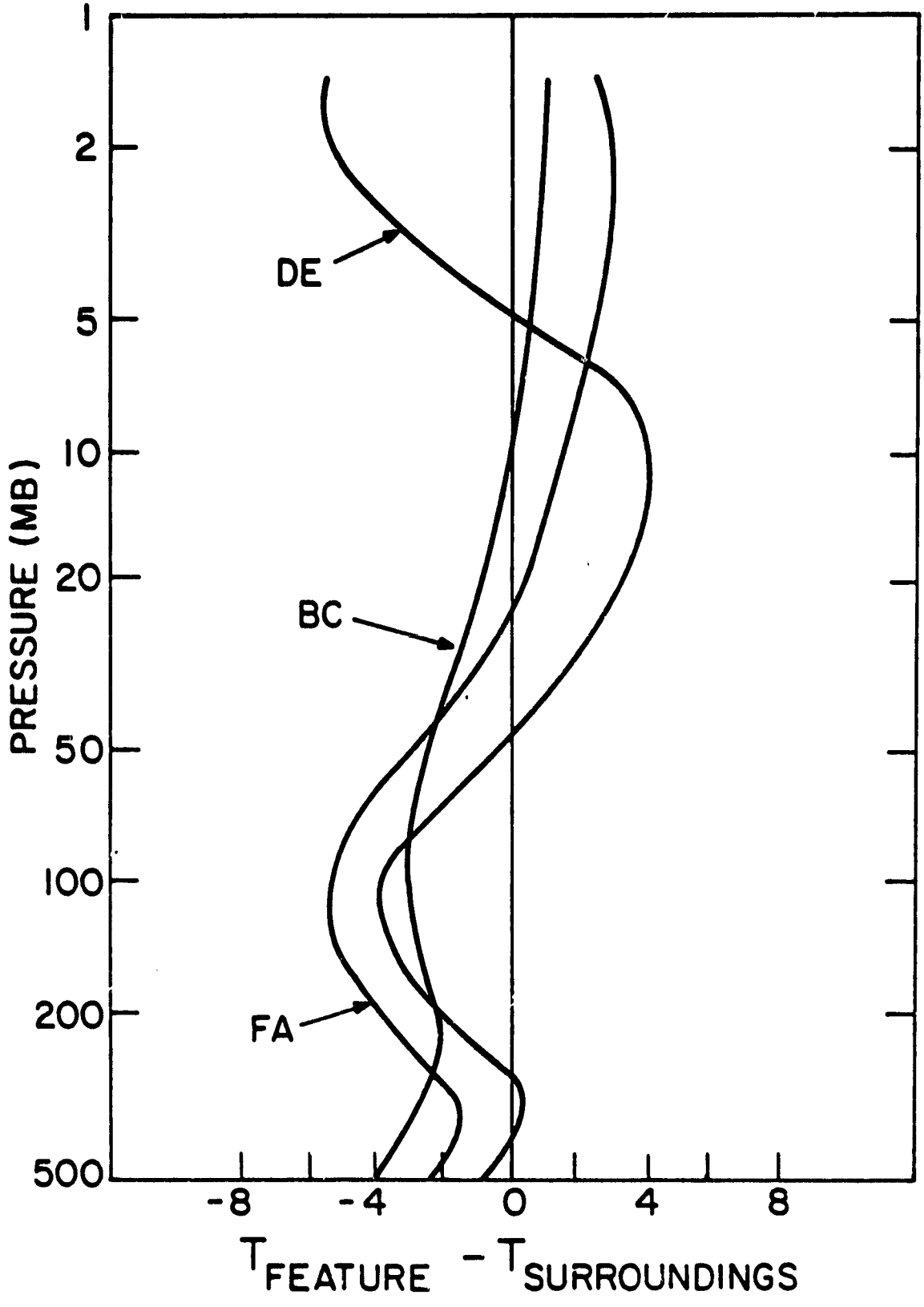
1
2
5
10
20
50
100
200
500
PRESSURE (MB)
DE
BC
FA
-8
-4
0
4
8
T FEATURE - T SURROUNDINGS

Figure 1

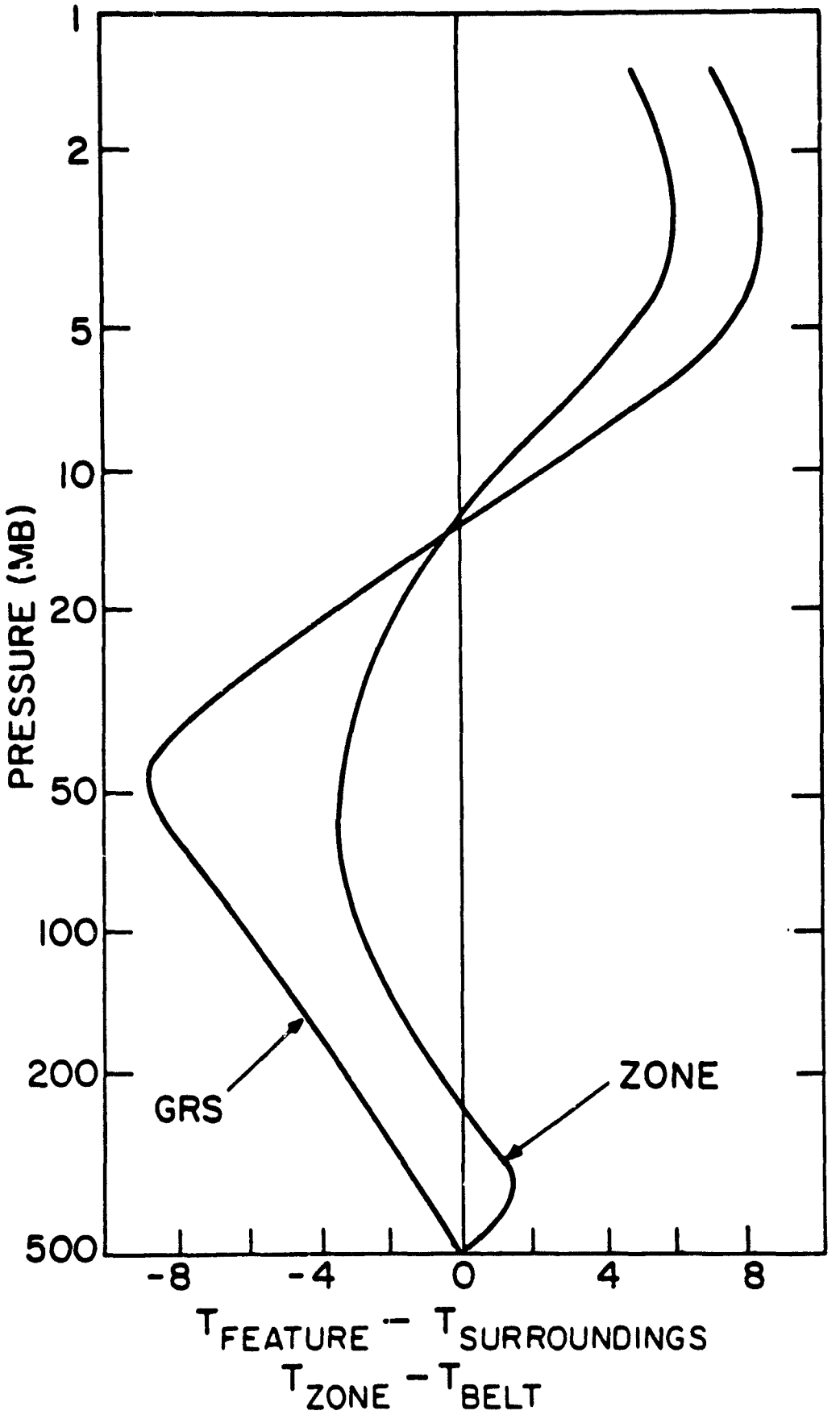
1
2
5
10
20
50
100
200
500
PRESSURE (MB)
GRS
ZONE
-8
-4
0
4
8
T FEATURE − T SURROUNDINGS
T ZONE − T BELT

Figure 2

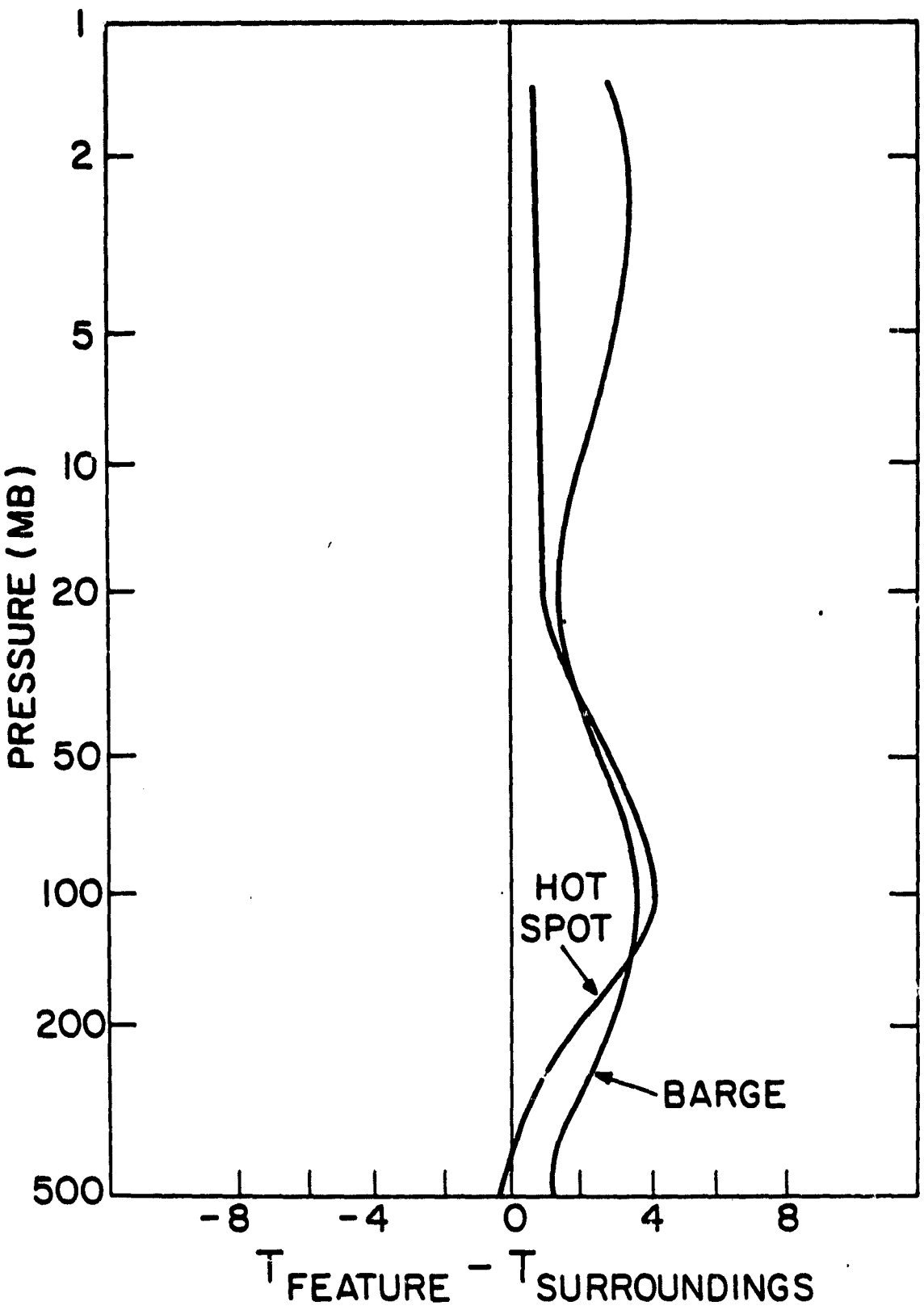
1
2
5
10
20
50
100
200
500
PRESSURE (MB)
HOT
SPOT
BARGE
-8
-4
0
4
8
T FEATURE - T SURROUNDINGS

Figure 3

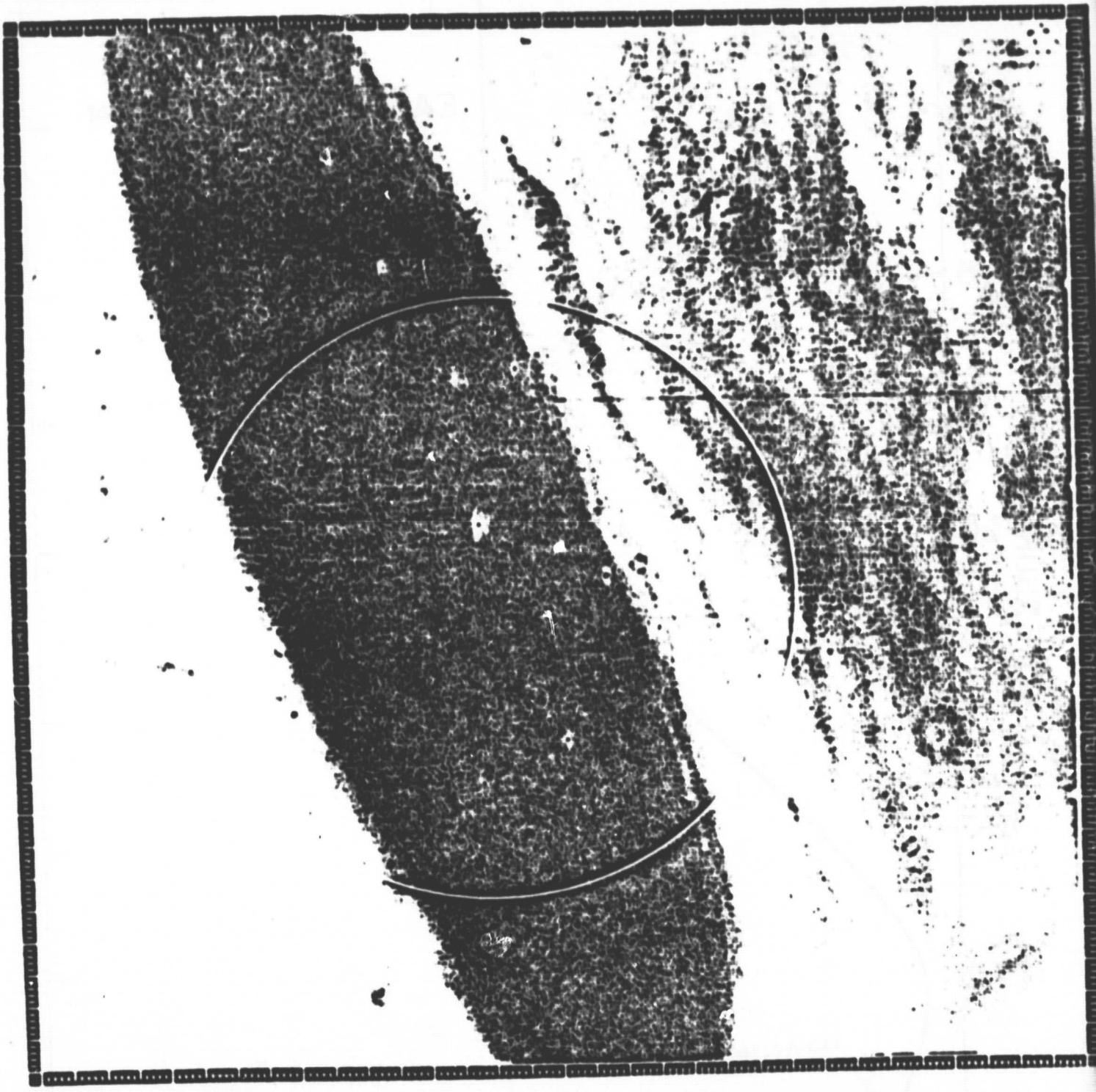

Figure 4

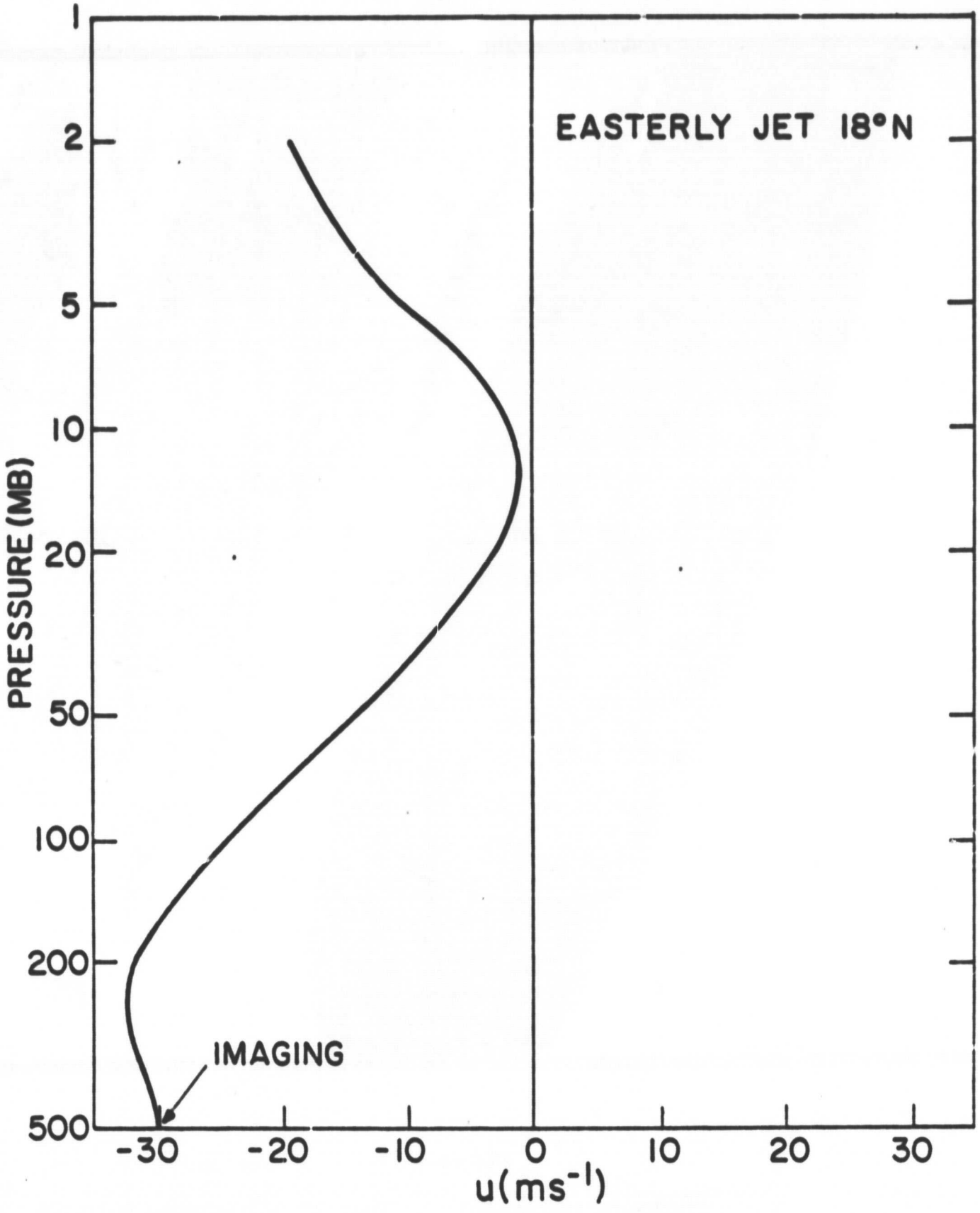
EASTERLY JET 18°N
PRESSURE (MB)
1
2
5
10
20
50
100
200
500
IMAGING
-30
-20
-10
0
10
20
30
u(ms⁻¹)

Figure 5